European Journal of Cell Biology 102 (2023) 151317

Contents lists available at ScienceDirect

European Journal of Cell Biology

journal homepage: www.elsevier.com/locate/ejcb

Riluzole treatment modulates KCC2 and EAAT-2 receptor expression and Ca^{2+} accumulation following ventral root avulsion injury

Krisztián Pajer [a], Tamás Bellák [a], Tímea Grósz [c,1], Bernát Nógrádi [b,e], Roland Patai [b], József Sinkó [c,2], Laurent Vinay [d], Sylvie Liabeuf [d], Miklós Erdélyi [c], Antal Nógrádi [a,*]

[a] Department of Anatomy, Histology and Embryology, Albert Szent-Györgyi Medical School, University of Szeged, Szeged, Hungary
[b] Institute of Biophysics, Biological Research Centre, Szeged, Hungary
[c] Department of Optics and Quantum Electronics, Faculty of Science and Informatics, University of Szeged, Szeged, Hungary
[d] Institut de Neurosciences de la Timone, UMR 7289, CNRS and Aix Marseille Université, Campus Santé Timone, 13385 Marseille, France
[e] Department of Neurology, Albert Szent-Györgyi Health Center, University of Szeged, Szeged, Hungary

ARTICLE INFO

We dedicate this study to our friend and colleague, the late Laurent Vinay, who initiated this collaboration between the research groups in Szeged, Hungary and Marseille, France.

Keywords:
Calcium
EAAT-2
KCC2
Riluzole
Motoneuron injury

ABSTRACT

Avulsion injury results in motoneuron death due to the increased excitotoxicity developing in the affected spinal segments. This study focused on possible short and long term molecular and receptor expression alterations which are thought to be linked to the excitotoxic events in the ventral horn with or without the anti-excitotoxic riluzole treatment. In our experimental model the left lumbar 4 and 5 (L4, 5) ventral roots of the spinal cord were avulsed. Treated animals received riluzole for 2 weeks. Riluzole is a compound that acts to block voltage-activated Na^+ and Ca^{2+} channels. In control animals the L4, 5 ventral roots were avulsed without riluzole treatment. Expression of astrocytic EAAT-2 and that of KCC2 in motoneurons on the affected side of the L4 spinal segment were detected after the injury by confocal and dSTORM imaging, intracellular Ca^{2+} levels in motoneurons were quantified by electron microscopy. The KCC2 labeling in the lateral and ventrolateral parts of the L4 ventral horn was weaker compared with the medial part of L4 ventral horn in both groups. Riluzole treatment dramatically enhanced motoneuron survival but was not able to prevent the down-regulation of KCC2 expression in injured motoneurons. In contrast, riluzole successfully obviated the increase of intracellular calcium level and the decrease of EAAT-2 expression in astrocytes compared with untreated injured animals. We conclude that KCC2 may not be an essential component for survival of injured motoneurons and riluzole is able to modulate the intracellular level of calcium and expression of EAAT-2.

1. Introduction

Axonal injury close to the cell body, such as ventral root avulsion, causes the death of vast majority of damaged motoneurons (Gloviczki et al., 2017; Koliatsos et al., 1994; Nógrádi et al., 2007). The injured motoneurons become vulnerable to excitatory stimuli and only a minority of them survives the injury (Nógrádi and Vrbová, 2001; Pintér et al., 2010). Riluzole (2-amino-6-trifluoromethoxy-benzothiazole) is a potent molecule that acts to block voltage activated Na^+ and Ca^{2+} channels, activate K^+ channels and inhibit presynaptic glutamate release (Doble, 1996). Moreover, riluzole is able to rescue around 70% of the injured motoneurons, if the treatment is started within 10 days after the avulsion injury and reduces the damage to neurons caused by ischemia in the spinal cord, too (Gloviczki et al., 2017; Lang-Lazdunski et al., 1999; Nógrádi et al., 2007).

Excitatory amino acid/glutamate transporters of astrocytes are responsible for clearing extracellular glutamate from synaptic environment. The glial glutamate transporter-2 (EAAT-2) proteins are mainly

Abbreviations: ALS, amyotrophic lateral sclerosis; dh, dorsal horn; EDDs, electron-dense deposits; EAAT-2, glial glutamate transporter-2; KCC2, K^+–Cl^-cotransporter-2; lvh, lateral ventral horn; mvh, medial ventral horn; NMDA, N-Methyl-D-aspartic acid; riluzole, (2-amino-6-trifluoromethoxy-benzothiazole); vf, ventral funiculus.

* Correspondence to: Department of Anatomy, Histology and Embryology, Albert Szent-Györgyi Medical School, University of Szeged, Kossuth Lajos sgt. 38, H-6724 Szeged, Hungary.
E-mail address: nogradi.antal@med.u-szeged.hu (A. Nógrádi).
[1] Present address: ELI-ALPS Research Institute, Szeged, Hungary.
[2] Present address: Mediso Medical Imaging Systems, Budapest, Hungary.

https://doi.org/10.1016/j.ejcb.2023.151317
Received 26 July 2022; Received in revised form 18 April 2023; Accepted 19 April 2023
Available online 20 April 2023

expressed in astrocytes (Rothstein et al., 1994). EAAT-2 is a major contributor to glutamate clearance to prevent neuronal excitotoxicity and hyperexcitability (Lauriat et al., 2007). The absence or down-regulation of EAAT-2 expression results in accumulation of glutamate in the synaptic cleft and glutamate receptor overstimulation which are associated with excessive influx of ions such as Ca^{2+} into the neurons (Kim et al., 2011). These processes occur despite the elimination of excitatory synapses from the surface of motoneurons whose axons have been avulsed or cut intramedullary in the spinal cord (Lindå et al., 2000; Spejo and Oliveira, 2015). The overload of intracellular calcium leads to the inappropriate activation of calpains and calcium-dependent proteases and eventually to an acceleration of the degenerative process of neurons (Rossi and Volterra, 2009). Dysfunction or reduced expression of EAAT-2 is seen in several neurological diseases, including stroke, amyotrophic lateral sclerosis (ALS) and epilepsy (Rothstein et al., 1992; Tanaka et al., 1997). In addition, many studies in animal models of neurological disorders indicated increased EAAT2 expression to provide a neuroprotective effect.

The K^+–Cl^-cotransporter-2 (KCC2) is a well-known member of the cation-chloride cotransporters and is expressed in the adult mammalian central nervous system. KCC2 plays a pivotal role in regulating the intracellular chloride ion homeostasis in healthy mature neurons (Blaesse et al., 2009). It is a main Cl^- extruder that uses the energy of the electrochemical K^+ gradient to transport Cl^-. The KCC2 protein is found to be associated with the plasma membrane in both somatic and dendritic compartments (Gulyás et al., 2001; Szabadics et al., 2006; Williams et al., 1999). Phosphorylation of the KCC2 residue Ser940 regulates KCC2 stability of the cell surface and thus is suggested to enhance KCC2 activity (Lee et al., 2007). The expression of KCC2 is reduced in several neurological disorders such as Huntington's disease, Rett syndrome and spinal cord injury, and the resulting slight increase in intracellular concentration of chloride ions, dramatically compromises the excitatory inputs and inhibitory transmissions (Dargaei et al., 2018; Doyon et al., 2011; Kahle et al., 2008; Lee et al., 2011; Prescott et al., 2006; Sánchez-Brualla et al., 2018). Under certain circumstances, increased N-methyl-D-aspartic acid (NMDA) receptor activity and associated Ca^{2+} influx have resulted in dephosphorylation of KCC2 Ser940, leading to loss of KCC2 function and increased neuron excitability, including motoneurons located caudal to the level of spinal cord injury (Boulenguez et al., 2010; Lee et al., 2011). Moreover, down-regulating the K^+-Cl^- co-transporter KCC2 reduces GABAergic inhibition and supposedly may lead to spasticity after spinal cord injury (Plantier et al., 2019).

On the other, distal axotomy of motoneuronal axons with perikaryal locations in the brainstem or spinal cord results in temporary down-regulation of KCC2 expression along with the disappearance of KCC2 from the cell membrane associated with altered cytoplasmic KCC2 trafficking (Kim et al., 2018; Mòdol et al., 2014; Tatetsu et al., 2012). Other studies that applied in situ hybridization to detect KCC2 mRNA revealed a significantly less prevalent KCC2 production in the axotomized vagal and facial neurons (Nabekura et al., 2002; Toyoda et al., 2003). These findings were later confirmed by a more recent study concerning spinal motoneurons (Akhter et al., 2019). However, these axotomies performed distal to the perikaryon of the motoneuron do not lead to considerable cell loss. In contrast, majority of the motoneurons with avulsed axons are destined to die likely due to multifactorial causes, out which excitotoxicity and related intracellular Ca^{2+} overload appear to be the major factors leading to cell death.

Despite the vast information available on injured motoneurons suffering from a distal axotomy, little is known about the relationship and mutual actions of intracellular calcium level and expression of EAAT-2 in the affected spinal segment. Moreover, alterations of cytoplasmic and membrane-bound KCC2 expression and possible down-regulation of that in injured motoneurons following ventral root avulsion has not been studied yet. It appears feasible to obtain an overview of changes of these important pathoregulatory components in a wide time window following central motoneuron injury. It is likely, although not clarified yet, that intracellular calcium overload and EAAT2 expression may play an important role in the outcome of severe motoneuron injury. On the other hand, it is not obvious whether a proximal axotomy induced more sever changes of the KCC2 expression in the injured motoneurons, than a distal, non-fatal axotomy. The aim of the present study was to find out whether (1) ventral root avulsion influences the intracellular calcium level, EAAT-2 and KCC2 expression in the affected spinal segments in a time dependent manner; (2) riluzole is able to influence any of these changes after the injury even if the damaged motoneurons have no opportunity to regenerate their axons.

2. Materials and methods

2.1. Statement of ethical approval

The experiments were carried out with the approval of the National Food Chain Safety Office, Hungary regarding the care and use of animals for experimental procedures (I./1569/2019). All the procedures were carried out according to the Helsinki Declaration on Animal Rights. Adequate care was taken to minimize pain and discomfort. Efforts were made to minimize the number of animals used.

2.2. Surgical procedure

Altogether 48 Sprague–Dawley rats (weight at time of surgery: 220–250 g) were used in this study and divided in 2 experimental groups. In control (surgery without treatment) the left L4-L5 ventral roots were avulsed from the cord (*AV* group, n = 24). These animals were injected with vehicle (PBS) only. In the other group (*AV+RIL* group, n = 24) the same surgical procedure was performed the animals were treated with riluzole for 2 weeks. The operated animals survived for 5, 7, 10, 16, 21 and 63 days (n = 4 in each group). All the operations were carried out in deep ketamine-xylazine anesthesia (ketamine hydrochloride (Ketavet), 110 mg/kg body weight; xylazine (Rompun) 12 mg/kg body weight) with sterile precautions. To maintain the body temperature at 37.0 ± 0.5 °C, the rats were kept on a temperature-controlled heating pad (Supertech Ltd.) during the surgery. Laminectomy was performed at the level of T13–L1 vertebrae, the dura was opened and the left L4 and L5 ventral roots were gently pulled out leaving the dorsal roots intact. The spinal cord was covered with the remaining dura, the wound was closed and the animals were allowed to recover. Animals received meloxicam (Metacam; 0,5 mg/kg body weight, Boehringer Ingelheim Vetmedica) for 3 days as postoperative treatment.

2.3. Riluzole treatment

Animals in the *AV+RIL* group were treated with Riluzole (kind gift of Tocris Cookson Ltd., 4 mg/kg) for 2 weeks. Riluzole treatment started immediately after the surgery. The drug was injected intraperitoneally daily for 1 week and then every second day for the next 1 week. This treatment protocol was based on the successful riluzole treatment described in our earlier paper (Gloviczki et al., 2017; Nógrádi et al., 2007; Pintér et al., 2010). The dose of riluzole was established from data obtained from our earlier and other laboratories' experiments (Maltese et al., 2005; Nógrádi and Vrbová, 2001; Schwartz and Fehlings, 2001).

2.4. Immunohistochemistry

Operated animals survived for 5, 7, 10, 16, 21 and 63 days and were deeply re-anaesthetized as described above and perfused transcardially with saline (0.9% NaCl) followed by 4% paraformaldehyde in 0.1 M phosphate buffer (pH=7.4). The lumbar part of the spinal cords was removed and kept in the same fixative for 24 h. The tissues were then immersed in 30% sucrose solution in PBS. Parallel 25 μm-thick cryostat

sections were cut on a Leica CM1850 cryostat (Leica) and mounted on gelatinized slides.

The sections were preincubated in 3% bovine serum albumin (BSA, Sigma-Aldrich) in PBS for 1 h at room temperature. Primary antibodies were used to treat the sections overnight at 4 °C as follows: rabbit anti-KCC2 (1:200; Merck-Millipore, 07–432), rabbit anti-pKCC2 (1:200, Thermo Fisher Scientific, PA5–95678), mouse anti-beta(III)-tubulin (TUBB3, 1:500; Abcam, ab7751), goat anti-ChAT (1:50, Sigma-Aldrich, AB144P), rabbit anti-VAChT (1:200, Synaptic Systems, 139 103) and rabbit anti-EAAT-2 (1:500, Abcam, ab205248). After washing in PBS (3 ×5 min), the immune reaction was completed by goat anti-rabbit AlexaFluor (AF) 488 (1:600, Thermo Fisher Scientific, A11008), goat anti-rabbit AF 594 (1:600, Thermo Fisher Scientific, A-11012), goat anti-rabbit AF 647 (1:600, Thermo Fisher Scientific, A27040), donkey anti-rabbit AF 488 (1:600, Thermo Fisher Scientific, A21206), donkey anti-mouse AF 594 (1:600, Thermo Fisher Scientific, A21203) or donkey anti-goat AF 594 (1:600, Thermo Fisher Scientific, A11058). The sections were covered with Vectashield mounting medium (Vector Laboratories). Negative controls for the secondary antibodies were performed by omitting the primary antibodies.

Sections were photographed using an Olympus DP74 digital camera and CellSens software (V1.18; 149 Olympus Ltd.) mounted on an Olympus BX51 fluorescence microscope (objectives: 20 ×0.50 NA; 40 ×0.75 NA, Olympus Ltd.) and a compact confocal microscope (objective: 60 ×1.35 NA; Olympus) with Fv10i software (V2.1; Olympus Ltd.).

2.5. Cell counts

The numbers of VAChT+ motoneurons in the ventral horn were determined on every fifth cryostat section in the ventral horn of L4 and L5 segments both at the injured and contralateral side. The number of VAChT+ motoneurons in the injured ventral horn was divided by the number of VAChT+ motoneuron in the uninjured contralateral ventral horn and multiplied by 100. This calculation gave the rate of surviving motoneuron after avulsion injury.

The KCC2-positive and KCC2-negative (evaluated after their KCC2 membrane positivity) motoneurons were analyzed at high magnification. The motoneurons were identified in the affected ventral horns by the typical large size, the location within the ventral horn and ChAT immunostaining. The number of KCC2 membrane-positive motoneurons was determined. This number was divided by the number of motoneurons (summation of KCC2-negative + KCC2-positive motoneurons) of injured ventral horns and multiplied by 100.

2.6. Confocal image and data analysis

Spinal cord sections were immunostained under identical conditions and then imaged with a confocal microscope (FluoView® FV10i-W, Olympus Ltd.). To quantify the immunohistochemical staining pattern, 1 μm-thick serial optical sections were created with the 10x objective by using 1.5x zoom. Intensity measurements were made (ImageJ, NIH) from every fifth section from four different regions within the L4 and L5 segments: the lateral ventral horn (lvh), the ventral funiculus (vf), the medial ventral horn (mvh) and the region comprising laminae I–II of the dorsal horn (dh). Mean pixel intensities at different survival times were normalized to the uninjured contralateral side on the same section.

2.7. Sample preparation for dSTORM imaging

Before STORM imaging, the sample was incubated in STORM switching buffer for 10 min at room temperature. After the incubation phase the buffer was replaced with fresh medium and the sample was covered with a glass #1.5 coverslip (WillCo Wells B.V.). To minimize the thickness of the sample medium the microscope slide and the coverslip were gently pushed together. This reduced distance ensured the proper operating conditions of the Nikon Perfect Focus System. The sample was then sealed with a two-component silicone adhesive and placed on the microscope stage.

2.8. Super-resolution imaging

All dSTORM super-resolution experiments were performed on a custom-built inverted microscope based on a Nikon Eclipse Ti-E frame under EPI illumination at an excitation wavelength of 647 nm (MPB Communications Inc.: 647 nm, P_{max}=300 mW). The laser power, controlled via an acousto-optic tuneable filter, was set to 4 kW/cm ^{2} on the sample plane. Additional lasers operating at 405 nm (Nichia: 405 nm, 60 mW) and 561 nm (Cobolt Jive 561 nm, 300 mW) were used for reactivation and reference measurements, respectively. Images were captured by an Andor iXon3 897 BV EMCCD digital camera (512 × 512 pixels with a pixel size of 16 μm). Frame stacks for dSTORM super-resolution imaging were captured at a reduced image size (crop mode), where only the central, 128 × 128 pixels region was selected. However, the actual size of the cropped area changed from sample to sample depending on the shape and size of the selected cells. Typically, 10,000 frames were captured with an exposure time of 30 ms. Reference images with a full field of view were captured at low intensity when the majority of fluorescent molecules were still active, and the overall structure of the labelled sample could be visualized. Because of the reduced volume, the switching buffer could provide ideal photochemical conditions only for a limited period of time (~2 h). Whenever the imaging process required more time, the switching buffer was replaced. The captured and stored image stacks were evaluated and analysed by the rainSTORM localization MATLAB software (Sinkó et al., 2014). Localizations were filtered via their intensity, ellipticity and standard deviation values. Only the localizations with precisions of < 45 nm were used to form the final image. The estimated mean precision of the accepted localizations was around 20 nm. Drift introduced either by the mechanical movement of the sample or thermal effects was analyzed and reduced by means of a blind drift correction algorithm. Spatial coordinates of the localized molecules were stored, and the final super-resolved image was visualized. The multicolor merged images were generated by ImageJ software.

2.9. Cluster analysis with density-based spatial clustering of applications with noise

A density-based spatial clustering of applications with noise-based (DBSCAN) cluster analysis module implemented into the rainSTORM program was used for further quantitative evaluation. This algorithm requires two input parameters: a minimum number of points that form a cluster (N_{core}) and the maximum distance between two adjacent points (ε). After the reconstruction of the high-resolution image, the user can select a region using the box tracking tool, and set the two cluster analysis parameters (N_{core}, ε). The program plots and saves data for further evaluation and visualization. Larger areas (entire cells etc.) can also be selected, but the code automatically segments them into smaller regions to avoid computation failure. To eliminate the influence of non-specific labeling and imprecise, out-of-focus localizations, the high-resolution images were further filtered by keeping only the localizations with 25 nm precision. After thorough tests N_{core} and ε were set to 5 and 25 nm, respectively. All together 307 cells were evaluated and three, non-overlapping regions were selected and analysed with DBSCAN in each cell. The retrieved cluster numbers were normalised to a 20 × 20 pixel, ie. to a 10.24 μm^2 area in order to compare the results obtained for the treated and untreated samples. From the 307 cells 180 had signal also in their membranes, while the rest showed expression only in the cytoplasm.

2.10. Membrane analysis with Image J

The 180 cells having KCC2 expression also in their membranes were

analyzed by using the ImageJ program (NIH). The number of localizations in the selected membrane section was obtained as described below. Identically sized areas taken from both the membrane and cytoplams were used for analysis. As the next step, the difference between the mean intensity obtained in the case of the area containing the membrane and that of retrieved in the cytoplasm divided by two was calculated. This division was necessary since in the case of the membrane only half of analyzed area was inside the cell. Afterwards the mean intensity value retrieved this way was multiplied by the area of the selection, which gave a good estimate for the number of localizations in the analyzed rectangle. Since the dimensions of the selected rectangle were known, this value was normalized to length and thus the number of localizations in the selected membrane section was obtained.

2.11. Animals and tissue preparation for electron microscopy

AV and *AV+RIL* animals were sacrificed on postoperative day 5 or 10 (n = 3 animals from each treatment/each time point). Under terminal anesthesia, animals were transcardially perfused with 90 mM potassium oxalate (Merck-Millipore; pH adjusted to 7.4 with KOH) followed by 3% glutaraldehyde (Polysciences Inc.; pH adjusted to 7.4 with KOH) containing 90 mM of potassium oxalate (pH 7.4). Tissue samples were removed and fixed in the same fixative overnight (4 °C). Specimens were then rinsed in 7.5% sucrose (Molar Chemicals Kft.) containing 90 mM of potassium oxalate (pH 7.4), postfixed with 2% potassium pyroantimonate (Merck) + 1% osmic acid (Sigma-Aldrich; pH adjusted to 7.4 with acetic acid (Molar Chemicals Kft.) for 2 h (4 °C) as previously described (Borgers, 1981; Borgers et al., 1977; Meszlényi et al., 2020). Next, samples were rinsed in distilled water for 10 min, dehydrated in a graded series of ethanol, treated with propylene oxide, and embedded in Durcupan ACM epoxy resin (Sigma-Aldrich). Blocks were polymerized for 48 h at 56 °C. Semithin (0.3 μm) sections were cut from the blocks on an Ultracut UCT (Leica) ultramicrotome, etched, and stained (Maxwell, 1978; Richardson et al., 1960). Next, ultrathin sections (50 nm) were cut and mounted on single-hole formvar-coated copper grids, contrasted with uranyl acetate (2% in 50% ethanol) and lead citrate (2% in DW all from Electron Microscopy Sciences) (Reynolds, 1963; Wyffels, 2001).

2.12. Evaluation of the intracellular calcium level in the spinal cord motor neurons

Ultrathin sections were examined in a JEM-1400Flash transmission electron microscope (JEOL Ltd, Tokyo, Japan). Sections were screened at low magnification (400–1000x) to identify the anatomical boundaries and locate the motoneurons in the ventral horn. Ten images each representing the cytoplasmic region were taken from 10 motor neurons in each rat. Images were recorded as 16-bit grayscale images at an instrumental magnification of 12000x with a Matataki Flash (JEOL) 2kX2k high-sensitivity scientific complementary metal-oxide-semiconductor camera and saved in tagged image file format. The tissue preparation method, regularly used in our laboratory (Obál et al., 2006; Obál et al., 2019; Paizs et al., 2010), resulted in electron-dense deposits (EDDs) due to the precipitation of tissue calcium by the pyroantimonate-containing fixative. The relative volume of the EDDs representing the calcium precipitates which was determined by point counting methods (Mayhew, 1992), which was modified for these unique structures and photographic conditions (Obál et al., 2006). The pictures were analyzed with Image-Pro Plus image analysis software. First, the tessellation of sampling points was superimposed on each electron microscopic image, then sampling points hitting the perikaryal profile of individual motor neurons in each image served as reference areas and were counted. Sampling points hitting EDDs within the reference areas were counted, and expressed as percentages compared to the total number of sampling points superimposed on the reference area. The corresponding counts obtained in the individual fields were summed up throughout the series of the identified motor neurons in each animal, and the appropriate ratios expressing the relative amount of EDDs within these neurons were calculated for each animal. 10–10 motoneuronal cytoplasmic fields of view were analyzed in each animal (n = 3 / group), resulting in 30 evaluated images (and 30 corresponding motoneurons) in each experimental group. Furthermore, to validate the presence of these calcium deposits and their morphological differences

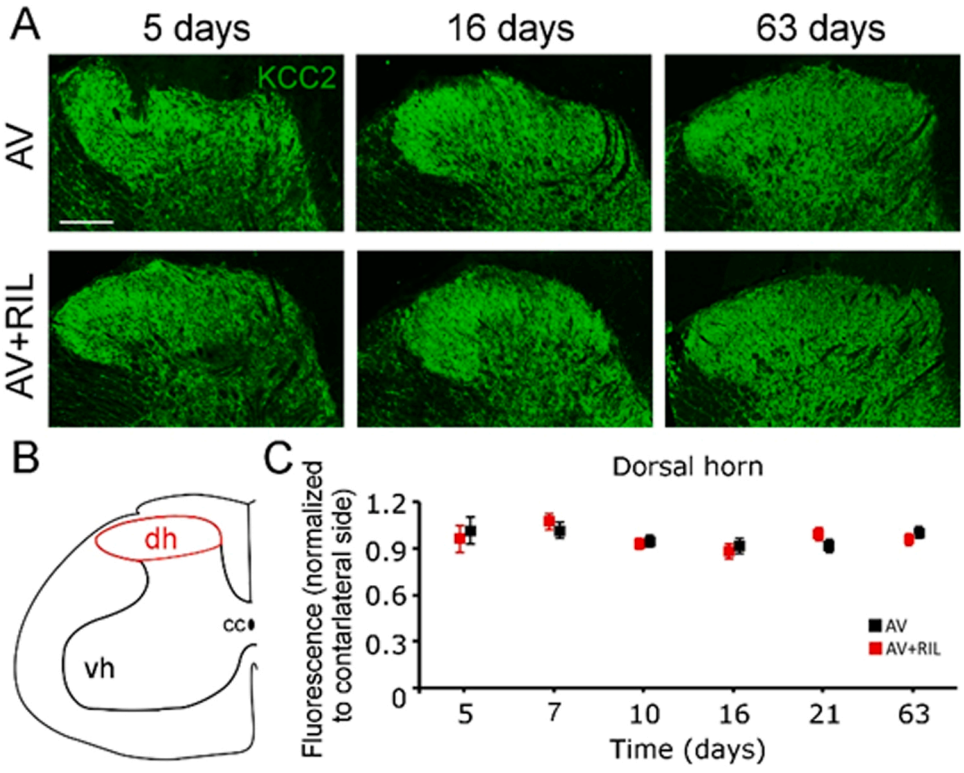

Fig. 1. Analysis of KCC2 expression in the dorsal horn of the L4–5 spinal segment from 5, to 63 days after the ventral root avulsion injury. (A) Confocal images showing KCC2 immunostaining in the dorsal horn of the L4 spinal segment on the affected side. (B) Labeling intensity was measured in the dorsal horn (dh, red-delineated area on the schematic drawing). (C) Diagram showing the mean fluorescence intensity in the dorsal horn of affected side that was normalized to uninjured contralateral side. KCC2 expression did not show any significant difference at various time points between the groups. vh: ventral horn, cc: central canal; Scale bar: 100 μm.

from ribosomes, energy-dispersive X-ray microanalysis was used. For this method, non-contrasted sections were prepared and the EDDs and ribosomes were examined in a transmission electron microscope operated at 120 kV, equipped with a Dry SD30GV SDD 30 mm2 X-ray detector (JEOL Ltd, Tokyo, Japan). X-ray spectra were recorded in the 0–40 keV energy range for 100 s, and were analyzed by the Visual Identification- and Thin Film Standardless Quantitative Analysis Programs of the JED-2300 Analysis Station (JEOL Ltd, Tokyo, Japan). The spectra from EDDs represented the presence of calcium and antimony in the appropriate energy range, while similar peaks were not visible if the areas of interest were the ribosomes (Fig. S1).

2.13. Statistical analysis

All statistical analyses were performed with R software (version 3.6.2) with R Studio Integrated Development Environment (version 1.1.453) for Windows. Data are reported throughout the manuscript as mean ± S.E.M. Two-sample t-test or One-way ANOVA with LSD post-hoc test was used to compare the group data. Relationships between cytoplasmic KCC2 and membrane bound KCC2 expression was determined by the Pearson correlation coefficient. The *p* value is given in the text and figure legends.

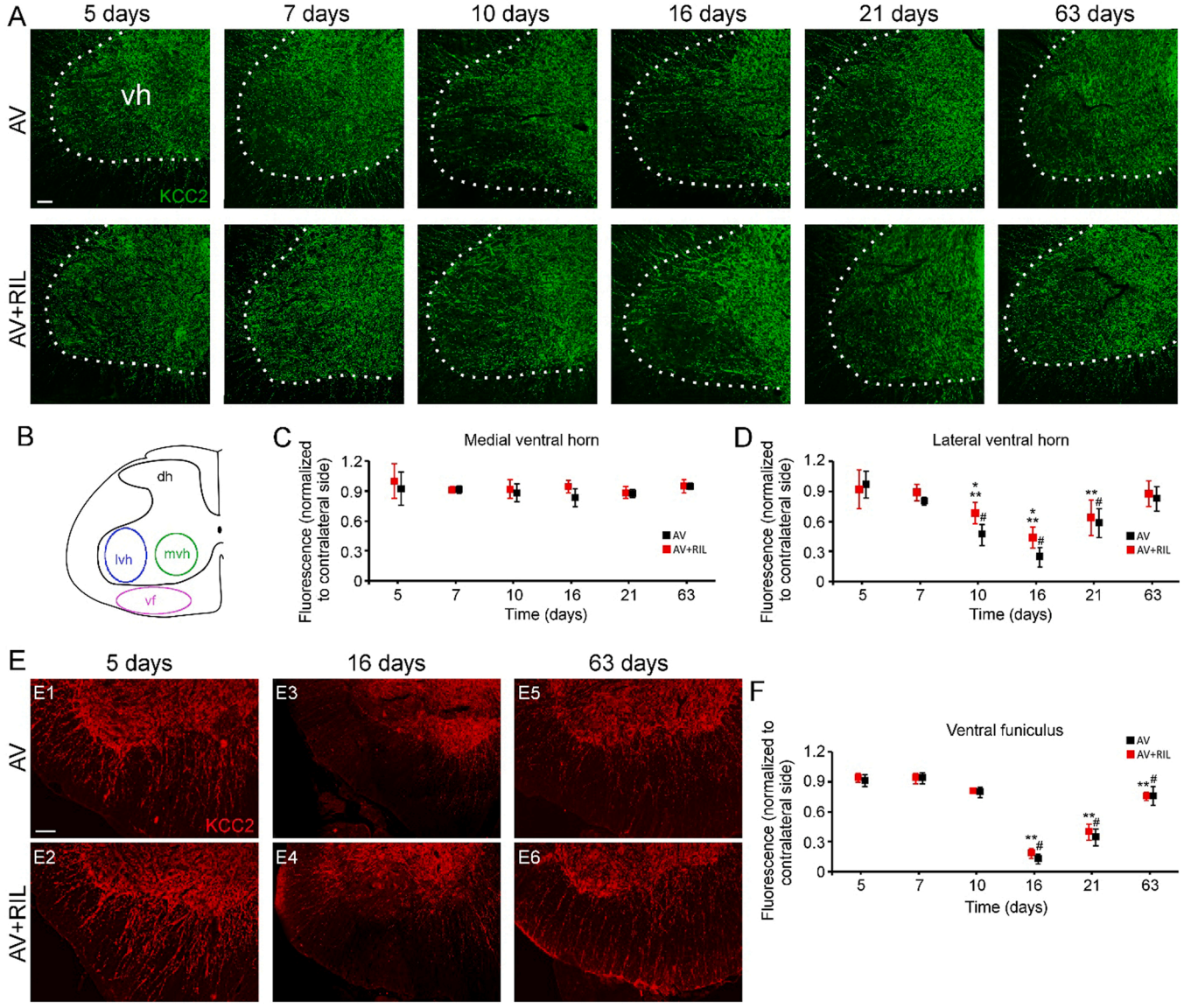

Fig. 2. Analysis of KCC2 expression in injured ventral lumbar spinal cord from 5 to 63 days after the ventral root avulsion injury. (A) Confocal images showing KCC2 immunostaining in the ventral horn (vh) of the L4 spinal segment on the affected side. (B) Labeling intensity was measured in the injured medial ventral horn (green circle, mvh), in the injured lateral ventral horn (blue circle, lvh) and in the ventral funiculus (purple circle, vf). (C) Mean fluorescence intensity was normalized to the uninjured contralateral side. KCC2 expression did not show any significant difference in medial grey matter. (D) Mean fluorescence intensity of KCC2 immunoreactivity showed a decrease from 10 days in the ventral horn and returned at day 63. Note that at days 10 and 16 it can be seen a significant difference between the groups. (E) Confocal images showing KCC2 immunostaining in the surrounding white matter of the L4 spinal segment at day 5 (E1, E2), at day 16 (E3, E4) and at day 63 (E5, E6) on the affected side. (F) Mean fluorescence intensity was normalized to the uninjured contralateral side. KCC2 immunoreactivity showed a decrease from 10 days and partly returned at day 63. dh: dorsal horn, cc: central canal; Two-sample t-test: * $p < 0.05$. at day 10 and 16 between *AV* vs. *AV+RIL* in D; One-way ANOVA with LSD post-hoc test: # $p < 0.01$ among AV 5 days, vs. AV 10, 16 and 21 days and * * $p < 0.01$ among *AV+RIL* 5 days vs. AV+RIL 10, 16 and 21 days in D; One-way ANOVA with LSD post-hoc test: # $p < 0.01$ among AV 5 days, vs. AV 16, 21 and 63 days and * * $p < 0.01$ among *AV+RIL* 5 days vs. *AV+RIL* 16, 21 and 63 days in F; Dashed lines indicate the border of grey matter and white matter. Scale bar in A: 50 μm and in E: 100 μm.

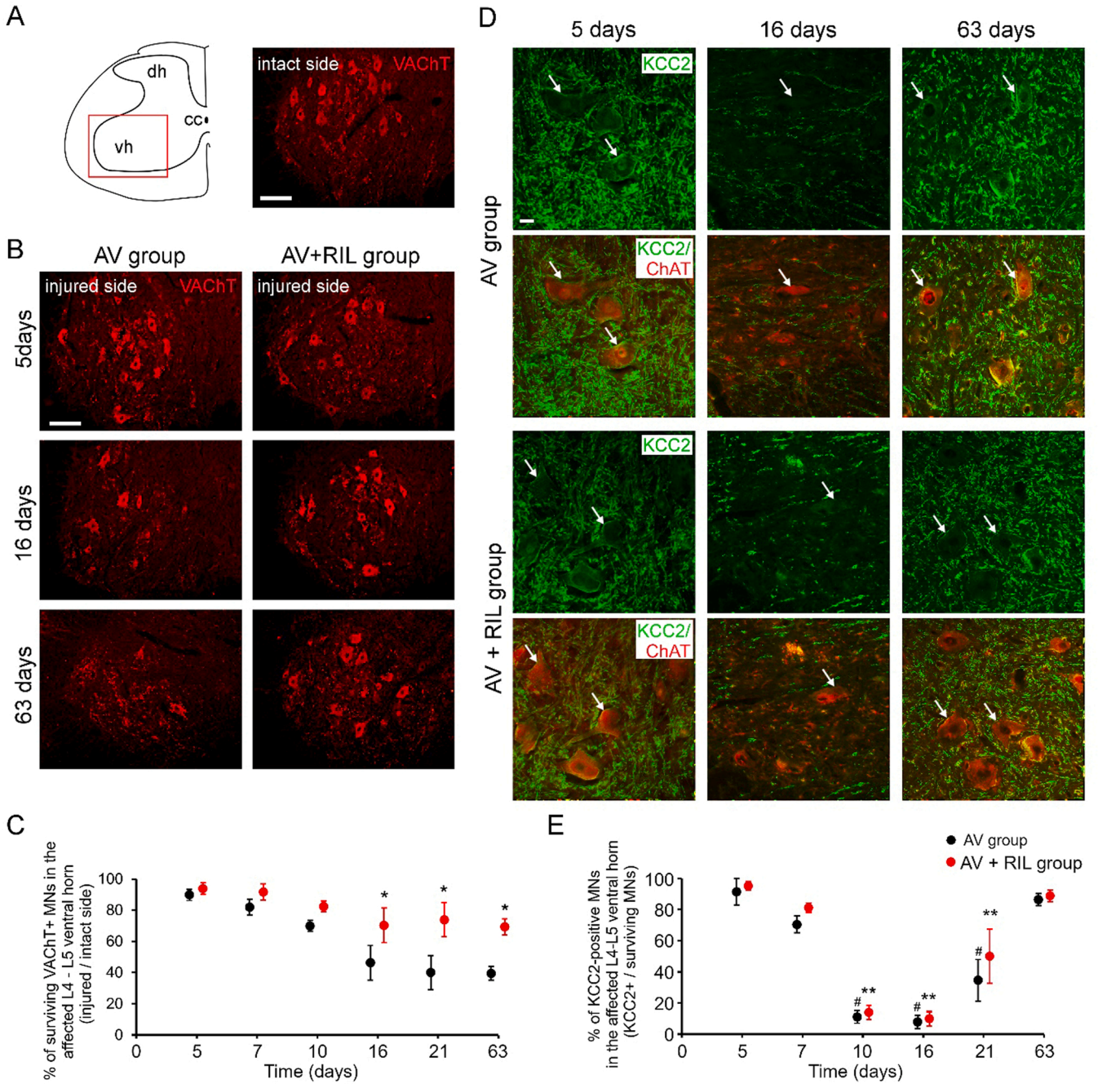

Fig. 3. Immunohistochemical localization of the VAChT and KCC2 in the injured motoneurons from 5, to 63 days after the injury. (A) Fluorescence image showing VAChT immunostaining in the contralateral ventral horn of the L4 spinal segment (red square on the schematic drawing). (B) Fluorescence images showing transverse sections of ventral horn from L4 spinal cord segment. (C) Bar graph displays the percentages of surviving (VAChT-positive) motoneurons compared to uninjured contralateral motoneuron numbers. Note the large numbers of surviving cells in the ventral horn in riluzole treated animal (*AV+RIL* group) 16 and 63 days after the injury. (D) KCC2 and ChAT immunostaining in the injured motoneurons at 5 days (D1; *AV* group), (D2; *AV+RIL* group), 16 days (D3; *AV* group), (D4; *AV+RIL* group) and 63 days (D5; *AV* group), (D6; *AV+RIL* group) after the injury. (E) Diagram displays the temporal changes of KCC2 expression in the membrane of ChAT-positive motoneurons. Expression of KCC2 decreased or disappeared in the membrane of vast majority of motoneurons on days 10, 16 and 21. Arrows show motoneurons in the injured ventral horns. dh: dorsal horn, cc: central canal, vh: ventral horn; Two-sample t-test: * $p < 0.05$ between *AV* vs *AV+RIL* at day 16, 21 and 63 in C; Two-sample t-test: * $p < 0.05$ between *AV* vs *AV+RIL* on day 7 and One-way ANOVA with LSD post-hoc test: # $p < 0.01$ among AV 5 days, vs. AV 10, 16 and 21 days and * * $p < 0.01$ among *AV+RIL* 5 days vs. *AV+RIL* 10, 16 and 21 days in E; Scale bar in A and B: 100 μm; in D1: 20 μm.

3. Results

3.1. Expression of KCC2 in the dorsal horn of the affected side after ventral root avulsion injury

In order to investigate the possible regional differences in KCC2 expression, we performed KCC2 immunohistochemistry at the L4 –L5 spinal level from 5 days to 63 days after L4-L5 ventral root avulsion. KCC2 labeling was analyzed and quantified in the dorsal spinal cord in the *AV* and the *AV+RIL* groups. At all experimental time points, the intensity of the labeling was normalized to that of the uninjured contralateral side. In the dorsal horn of the affected side, no visible difference of the immunostaining pattern as observed between the different groups (Fig. 1A). The KCC2 labeling was relatively stable at all time points.

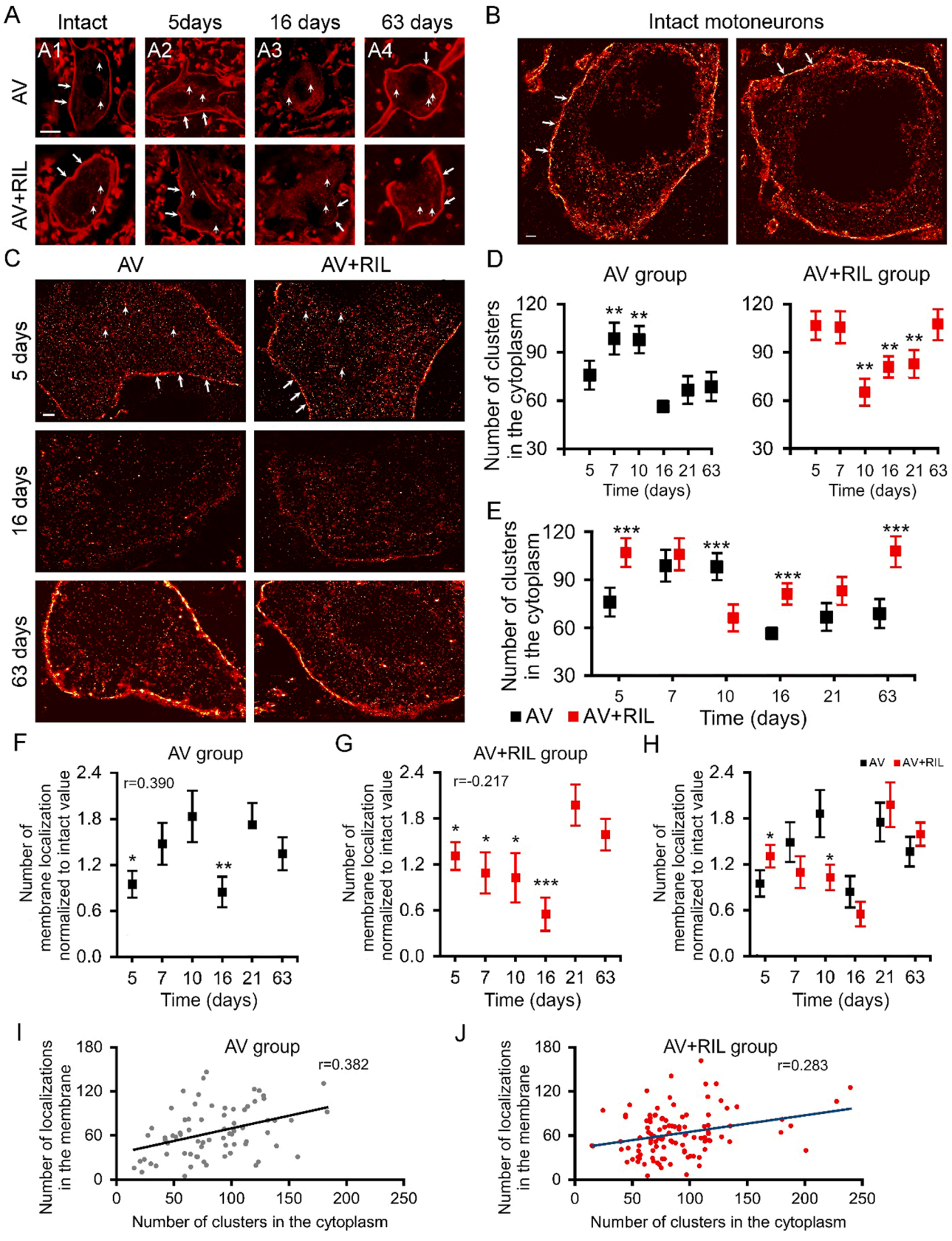

(caption on next page)

Fig. 4. dSTORM imaging and cluster analysis of injured motoneurons. Single optical confocal sections showing the KCC2 staining in motoneuron membranes of intact (A1), on day 5 (A2), on day 16 (A3) and on day 63 (A4) after the injury in both groups. (B) dSTORM images display organization and distributed pattern of KCC2 in intact and (C) injured motoneurons at different time points at nanoscale resolution in both groups. (D and E) Diagrams show the temporal changes of the number of clusters of KCC2 in the cytoplasm of motoneurons. (F-H) Diagrams showing the number of localizations in the membrane of injured motoneurons corresponding to KCC2 protein in the AV and AV+RIL group. (I and J) The number of localizations of KCC2 positively correlated with the number of clusters in the cytoplasm. Large arrows show the KCC2 staining in the membrane in A, B and C. Small arrows display KCC2 staining in the cytoplasm in A, B and C. One-way ANOVA with LSD post-hoc test: * * $p < 0.01$ among AV 7 and 10 days vs. *AV* 16, 21 and 63 days, *AV+RIL* 10 days vs. AV+RIL 5, 7 and 63 days, *AV+RIL* 16 and 21 days vs. *AV+RIL* 63 days in D, Two-sample t-test: * ** $p < 0.001$ between AV 5 days vs. *AV+RIL* 5 days, *AV* 10 days vs. *AV+RIL* 10 days, *AV* 16 days vs. *AV+RIL* 16 days and AV 63 days vs. *AV+RIL* 63 days in E; One-way ANOVA with LSD post-hoc test: * $p < 0.05$ among *AV* 5 days vs. AV 7, 10, 21 and 63 days, * * $p < 0.01$ among *AV* 16 days vs. *AV* 7, 10, 21 and 63 days in F, * $p < 0.05$ among *AV+RIL* 5, 7 and 10 days vs. *AV+RIL* 16, 21 and 63 days, * ** $p < 0.001$ among *AV+RIL* 16 days vs. *AV+RIL* 21 and 63 days in G, Two-sample t-test: * $p < 0.05$ between *AV* 5 days vs *AV+RIL* 5 days and *AV* 10 days vs. *AV+RIL* 10 days in H. Pearson correlation coefficient (r) can be seen in I and J. Scale bar in A: 10 μm; in B and C: 1 μm.

The quantitative analysis of the mean fluorescence in dorsal horn (*AV* and *AV+RIL* groups) revealed no significant expression pattern changes between the groups (Fig. 1B, C). The intensity slightly decreased, but remained stable at the time investigated.

3.2. Reduced expression of KCC2 in the ventral lumbar spinal cord

A dense and uniform KCC2 expression was found in both groups throughout the affected ventral horn 5 and 7 days after the injury. In contrast to the early time points, a weak staining was observed on days 10 and 16 in the injured ventral horn of both groups. The staining intensity started to increase on day 21 and returned to baseline intensity on day 63 (Fig. 2A). Next, we measured the mean fluorescence intensity of KCC2 expression in both lateral and medial compartments of the ventral horn at all examined time points (Fig. 2B-D). The expression of KCC2 only slightly decreased in the medial ventral horn and remained relatively stable in *AV* and *AV+RIL* groups (Fig. 2C). In contrast, a trend towards a reduction from day 7 to day 16 was observed in lateral ventral horn then a slight increase was observed at day 21 in both groups (Fig. 2D). Staining intensity was significantly stronger in the *AV+RIL* group on days 10 and 16 ($p < 0.05$ at day 10 and $p < 0.05$ at day 16) compared to *AV* group. The weakest expression of KCC2 in the lvh was measured at day 16 in both groups. It then returned and was stable at day 63 in both groups (Fig. 2D).

The labeled processes in both the grey and white matter are likely dendrites since KCC2 is not expressed in axons(Hübner et al., 2001; Stil et al., 2009). These dendrites in the white matter were densely labeled too, and could be followed towards the edge of the spinal cord on day 5 after the injury in both groups. Similarly, a strikingly different immunostaining pattern was observed between the different time points in the ventral funiculus (Fig. 2E). The most noteworthy feature of the labeling on day 5 was the presence of labeled processes in all directions into the ventral funiculus (Fig. 2E1 and E2). Only a faint labeling was observed in the ventral funiculus on day 16 (Fig. 2E3 and E4). In contrast, processes were labeled by KCC2 antibody and appeared to reach the edge of the spinal cord in the ventral funiculus on day 63 but the labeling intensity was not as strong as on day 5 (Fig. 2E5 and E6).

The fluorescence intensity of KCC2 labeling was quantified at each time point. The KCC2 expression was stable on days 5 and 7 after the injury in both groups, whereas a significant reduction was observed on days 16 and 21 ($p < 0.01$ among *AV* 5 days, vs. *AV* 16 and 21 days; $p < 0.01$ among *AV+RIL* 5 days vs. *AV+RIL* 16 and 21 days) after the injury. KCC2 intensity reached a relatively higher value on day 63 in both groups but was significantly weaker than earlier time points ($p < 0.01$ *AV* 5 days vs. *AV* 63 days and $p < 0.01$ *AV+RIL* 5 days vs. *AV+RIL* 63 days). No significant difference was observed in staining intensity between the *AV* and *AV+RIL* groups at the examined time points (Fig. 2 F).

3.3. Alteration of KCC2 expression in the close vicinity of the motoneurons

Our earlier study has shown that riluzole was able to rescue the vast majority of injured motoneurons after L4 ventral root avulsion (Nógrádi et al., 2007). VAChT immunohistochemistry was performed to detect the motoneurons in the injured and contralateral intact ventral horns (Fig. 3A and B). The morphological characteristics of the motoneurons were well preserved in the riluzole-treated group. In contrast, vast majority of the motoneurons in the *AV* group was not already found on day 63 after avulsion injury (Fig. 3B). Motoneurons were counted on the injured and contralateral sides of the ventral horn of the *AV* and *AV+RIL* groups from 5 to 63 days. Accordingly, the proportions of VAChT+ motoneurons on the operated side were similar in *AV* and *AV+RIL* groups 5 and 7 days after the injury. The proportion of VAChT+ motoneurons started to decrease in both groups from day 10 onwards, but significantly more motoneurons were missing in the *AV* group as compared to the *AV+RIL* group animals (Fig. 3C, at day 16 $p < 0.01$ between AV vs AV+RIL; at day 21 $p < 0.01$ between *AV* vs *AV+RIL*; at day 63 $p < 0.01$ between *AV* vs *AV+RIL*).

In the light of these results, we next investigated the KCC2 expression in the injured motoneurons. Co-labeling of KCC2 (in the cell membrane) with ChAT showed that the ratio of KCC2-expressing ChAT-positive motoneurons dramatically dropped by day 10 after avulsion injury in both experimental groups and remained low on the postoperative day 16, too (Fig. 3D and E). This marked drop of KCC2 was improved by the postoperative day 21 and restored to near normal level by day 63 (Fig. 3D and E).

The quantitative analysis of KCC2 membrane expression in the injured motoneurons revealed that significantly higher number of motoneurons expressed KCC2 in the plasma membrane on day 7 in the *AV+RIL* group ($p < 0.05$) compared to the *AR* group (Fig. 3E). In contrast, low number of motoneurons expressed KCC2 in their membrane at later time points ($p < 0.01$. *AV* 5 days vs. *AV* 10, 16 and 21 days and $p < 0.01$ *AV+RIL* 5 days vs. *AV+RIL* 10, 16 and 21 days). On day 63, the membrane-bound expression of KCC2 recovered in the motoneurons of both groups.

Recent studies suggested that phosphorylation of KCC2 residues enhances its transporter function (Blaesse et al., 2009; Kahle et al., 2008). Accordingly, we have performed pKKC2 (phosphorylated form of KCC2) and ChAT double labelling to determine the ratio of ChAT-positive motoneurons that expressed pKCC2 in the perikaryal membrane. Surprisingly, no difference was found in the pKCC2 expression pattern of injured and riluzole-treated motoneurons as compared with that of the KCC2 membrane expression (see Fig. 3E and Fig. S2). It should be noted, however, that pKCC2 expression was not ubiquitous in intact motoneurons, approximately 65% of them was positive for pKCC2 (Fig. S2B and D). This ratio was maintained in the affected motor pools of both *AV* and *AV+RIL* animals (Fig.S2D).

3.4. Cluster analysis of KCC2 in the cytoplasm of injured motoneurons

The KCC2 immunolabeling in confocal images appeared as a uniform band in the motoneuron membrane on the intact side of the spinal cord. On day 5 following injury the damaged motoneurons maintained their strong membrane staining in both groups (Fig. 4A1–2), but the membrane labeling became discontinuous by day 16 after injury with a marked return of staining intensity several weeks later (Fig. 4A3–4).

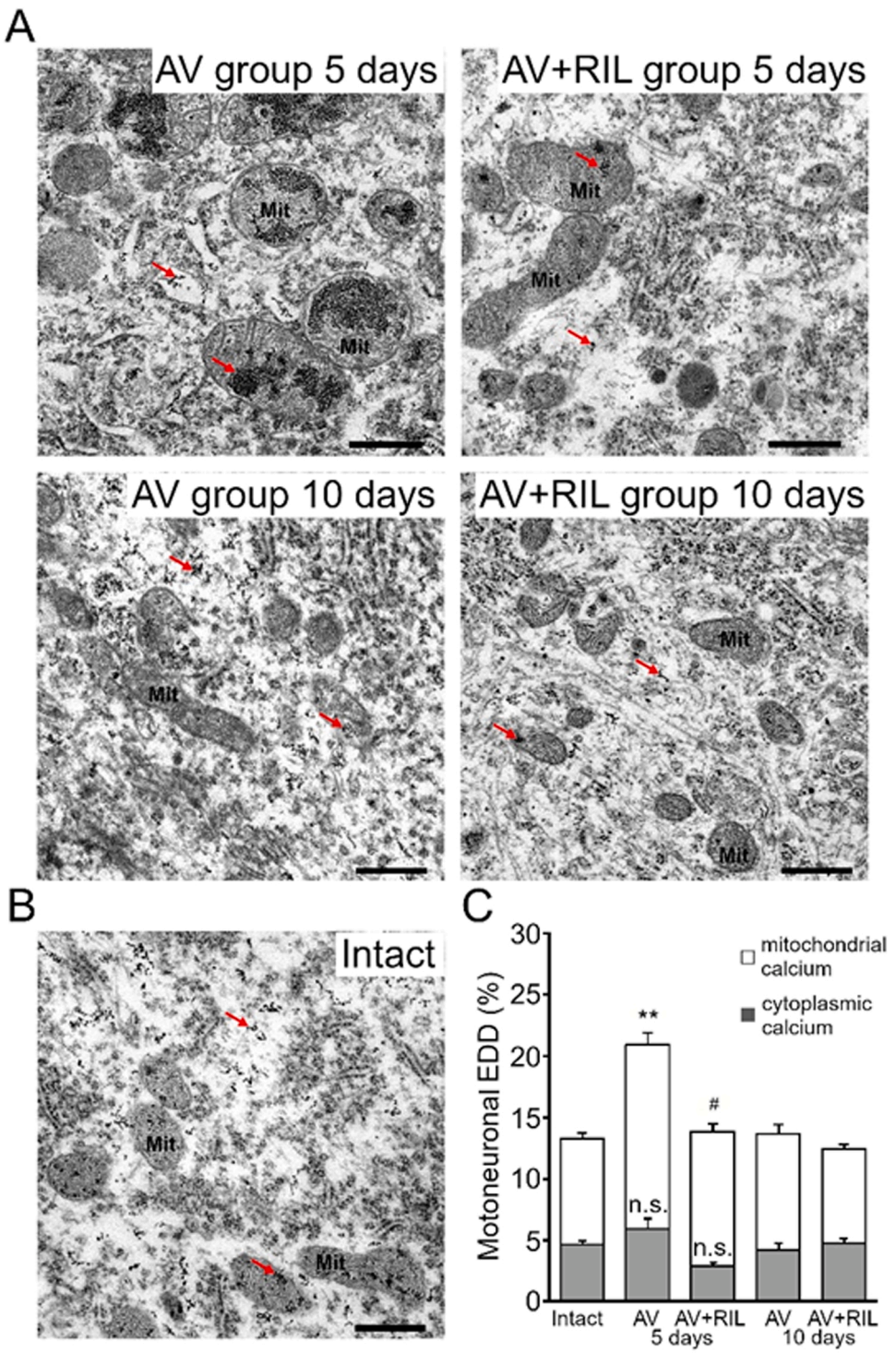

Fig. 5. Distribution of EDDs, representing the presence and amount of calcium in the cell body of injured motoneurons. Representative images obtained from perikaryal of injured motoneurons 5 and 10 days after injury in both groups (A). Perikaryal view of intact motoneurons is shown from the contralateral intact side (B). Quantitative analysis of changes of the EDDs in intact and injured motoneurons. Note the effect of riluzole treatment on the amount of calcium in the mitochondria of injured motoneurons 5 days after injury (C). One-way ANOVA with LSD post-hoc test: * * indicates $p < 0.01$ between intact (contralateral intact side) group vs. *AV* group at 5 days, # refers to $p < 0.05$ between *AV* group 5 days vs. *AV+RIL* group 5 days; Red arrows indicate small clusters of EDDs. n.s. = no significant difference between intact vs. *AV* group 5 days and *AV* 5days vs. *AV+RIL* 5 days group in cytoplasmic calcium level; Mit = mitochondrium; Scale bars: 500 nm.

KCC2-positive labeling was also observed in the cytoplasm of motoneurons with varying intensity in both groups.

To investigate the dynamics of KCC2 expression in the injured motoneurons the dSTORM technique of super resolution microscopy was applied. Detailed KCC2 organization pattern was observed in dSTORM images both in the cytoplasm and membrane of intact and injured motoneurons at various time points in different experimental groups (Fig. 4B and C, Fig. S3). KCC2 was found to aggregate into dense homogeneous clusters without clear boundaries in the cytoplasm of intact and injured motoneurons (Fig. 4B and C, Fig. S3). In order to investigate possible differences in cytoplasmic KCC2 expression, we quantified the number of KCC2 + clusters in the cytoplasm of injured motoneurons. The quantitative analysis of the KCC2 cluster expression dynamics revealed a significant increase of the clusters on days 7 and 10 followed by a sudden drop on day 16 in the *AV* group. After this time point a relatively low cluster number was observed in this group until day 63 (Fig. 4D). In contrast, animals who receive riluzole treatment showed high cytoplasmic cluster numbers on days 5 and 7, followed by a similar drop on day 10 and continuous recovery of cluster formation afterwards (Fig. 4D). Fig. 4E compares the dynamics of cluster deterioration and

reorganization in the AV and *AV+RIL* groups. The cluster density in *AV+RIL* group was significantly higher on days 5, 16 and 63 compared with the *AV* group suggesting a better compensatory mechanism in the early phase after injury and faster and more complete recovery of KCC2 cluster densities (Fig. 4E). In contrast, significantly decreased number of clusters could be detected at day 10 after injury in the riluzole treated group compared to *AV* group (Fig. 4E).

3.5. Analysis of KCC2 expression in the membrane of injured motoneurons

In the light of above results, we next investigated the issue of the KCC2 expression in the membrane of injured motoneurons. Only those motoneurons were analyzed which possessed KCC2 immunoreactivity in the membrane. A marked increase was followed by a sudden decline of number of localizations in the membrane of injured motoneurons of *AV* group in the first 16 days after the injury (Fig. 4 F). The statistical analysis showed that a significant trend towards an increase of KCC2 expression was observed from the fifth day to the tenth day ($p < 0.05$; n = 13 on day 5, n = 19 on day 7, n = 9 on day 10, r = 0.390; Pearson's correlation). Considering all time points, significantly lower number of localizations could be detected on days 5 and 16 after the injury. In contrast, riluzole treatment continuously and remarkably induced a decrease of the number of localizations for 16 days after injury (Fig. 4 G, $p < 0.05$; n = 32 on day 5, n = 18 on day 7, n = 18 on day 10, n = 8, r = 0.217; Pearson's correlation). It is notable that a significant increase of number of localizations could be observed on days 21 and 63 (Fig. 4 G). Significantly higher number of localizations was detected on day 5 in the *AV+RIL* group compared with the *AV* group (Fig. 4H). The number of localizations of KCC2 was, however, significantly lower 10 days after the injury in the *AV+RIL* group compared with the *AV* group (Fig. 4H).

We hypothesized that there may be a link between the cytoplasmic and membrane expressions of KCC2. Indeed, we found that the data cumulated form all time points were positively correlated regardless (Fig. 4I and J, *AV* group: $p < 0.05$; n = 72, r = 0.390; *AV+RIL* group: $p < 0.05$; n = 108, r = 0.283; Pearson's correlation). These results suggest that translocation of KCC2 to the somatic membrane of injured motoneurons increased when the level of cytoplasmic KCC2 was elevated.

3.6. Quantitative analysis of intracellular calcium levels in spinal cord motoneurons

Motoneurons in the affected L4–5 segments were analyzed by electron microscopy 5 and 10 days after the injury (Fig. 5). Qualitative electron microscopic examination of spinal cords from both experimental groups revealed mildly (in *AV+RIL* animals) and severely (*AV* animals) swollen mitochondria in injured motoneurons 5 days after the injury relative to intact motoneurons (Fig. 5A and B). Closer inspection showed an increased number of EDDs in the mitochondria in the spinal cords in the *AV* group, compared to intact or treated animals (*AV+RIL* group), at 5 days after the injury, which suggests the presence of an increased amount of Ca^{2+} in the mitochondria of untreated animals (*AV* group 5 days). The slight swelling of mitochondria ceased at day 10 after the injury in the treated group (*AV+RIL* group 10 days; Fig. 5A), while disruption of mitochondrial integrity, e.g. broken mitochondrial outer membranes was noticed in motoneurons of the untreated group (*AV* group 10 days; Fig. 5A). Next, we quantitatively analyzed the intracellular calcium level in the injured and intact motoneurons. Intracellular

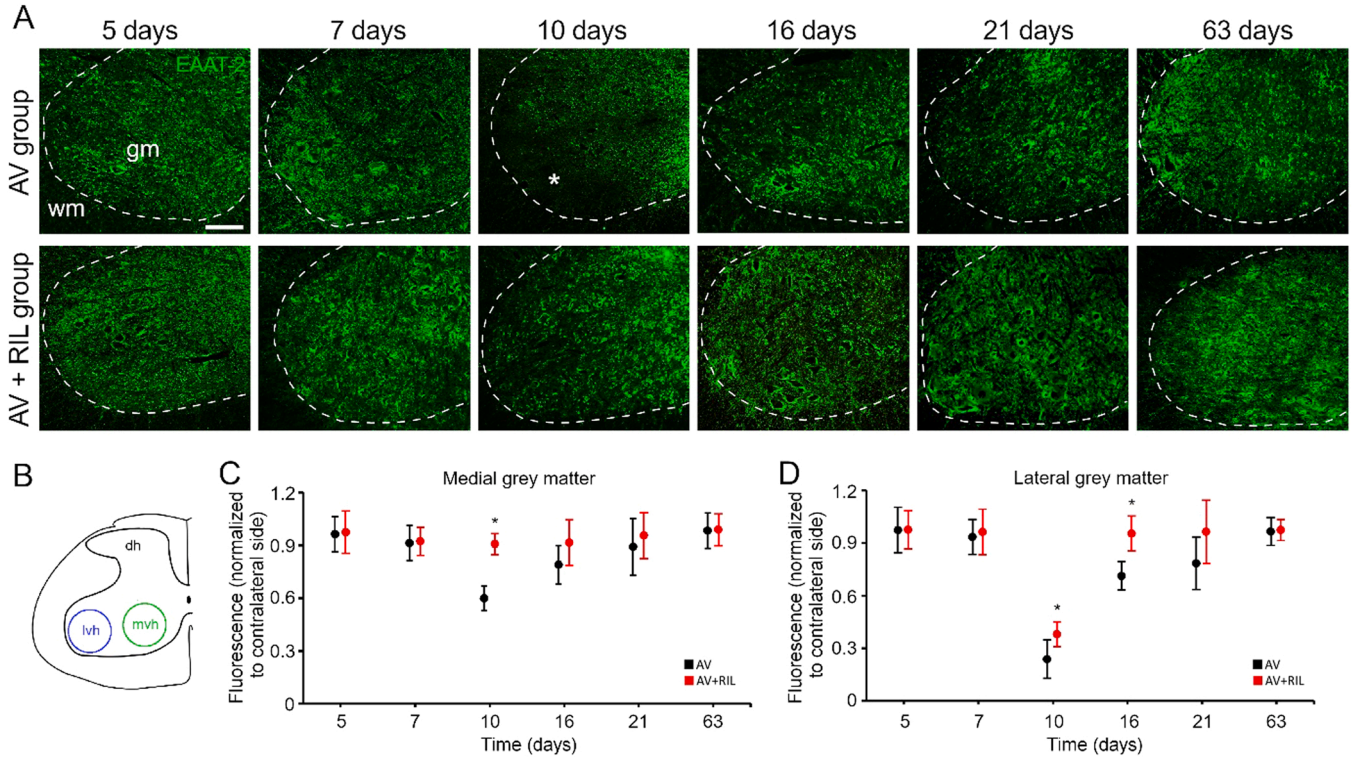

Fig. 6. EAAT-2 expression in injured ventral horn. (A) Reduced EAAT-2 densities are shown in the L4 spinal segment of *AV* and *AV+RIL* animals. (B) Labeling intensity was measured in the injured medial ventral horn (green circle, mvh) and in the injured lateral ventral horn (blue circle, lvh). (C) Mean fluorescence intensity of EAAT-2 immunoreactivity showed a reduction on day 10 after the injury in the medial grey matter of ventral horn in both groups. Note the significant difference between the groups on day 10. (D) Mean fluorescence intensity decreased significantly on day 10 and 16 after injury in the lateral grey matter of ventral horn in *AV* animals compared to *AV+RIL* animals. Dashed line shows the borderline between the white and grey matter. Two-sample t-test: * $p < 0.05$ between *AV* 10 days vs. *AV+RIL* 10 days in C and * $p < 0.05$ between *AV* 10 days vs. *AV+RIL* 10 days and *AV* 16 days vs. *AV+RIL* 16 days in D; abbreviations: gm = grey matter, wm = white matter; Asterisk indicates decreased EAAT-2 expression in the grey matter in A. Scale bar in A: 100 μm.

calcium level was expressed as an area occupied by the EDDs relative to the cytoplasmic/mitochondrial region of motoneurons. The quantitative evaluation revealed that avulsion of the ventral root resulted in a significant increase of mitochondrial calcium levels compared to the intact side 5 days after the injury in *AV* group ($p < 0.01$; Fig. 5C). Riluzole treatment could successfully prevent this increase ($p < 0.05$ between *AV* group 5 days vs. *AV*+*RIL* group 5 days). Ten days after the injury no significant increase could be detected on the injured side, thus the previously observed positive effect of riluzole treatment was no longer significant. It should be noted, that although mitochondria appeared very swollen 5 days after injury accompanied by strong accumulation of EDDs in them, their final disintegration was obvious only by day 10 after injury.

3.7. Riluzole treatment partially restores the EAAT-2 expression in injured ventral horn

It is well known that EAAT-2 is a pivotal contributor to neurodegeneration due to controlling balance between glutamate uptake and release in CNS (Ling et al., 2019). Therefore, we next investigated the expression of EAAT-2 in the injured ventral horn from 5 days up to 63 days after the avulsion injury in both animal groups. The labeling was dense throughout the ventral horn on day 5 but the staining intensity decreased on day 10 and returned broadly to basic level on day 21 after injury in both groups (Fig. 6A).

The quantitative analysis of mean fluorescence signal revealed that the EAAT-2 down-regulation in the riluzole-treated animals was considerably milder than in the controls. This restoring effect was more pronounced in the medial ventral horn compared with the lateral one (ventrolateral compartment of the ventral horn; Fig. 6 A, C and D). Expression of EAAT-2 was only minimally decreased in the medial ventral horn of the *AV*+*RIL* animals, but significant difference was detected only on day 10 between the treated and control groups (Fig. 6 C). In the lateral ventral horn the EAAT-2 expression markedly decreased on day 10 in both groups (Fig. 6D) but significantly higher reductions were measurable in *AV* animals compared with *AV*+*RIL* animals. In the *AV*+*RIL* group, expression of EAAT2 was restored on day 16, however, in the *AV* group it occurred more slowly (Fig. 6D).

4. Discussion

In the present study, we used a unilateral ventral root avulsion injury model to determine how axotomy of the axons of motoneurons close to the cell body at the L4–L5 spinal levels alters the processes leading to excitotoxicity including disturbed KCC2 and EAAT-2 expression as well as motoneuronal Ca^{2+} regulation in the affected segments. We showed here for the first time that a unilateral lumbar ventral root avulsion injury induced severe changes in the expression of ion/glutamate transporter molecules accompanied by mitochondrial Ca^{2+} accumulation. Moreover, riluzole treatment was able to positively modulate these changes, leading to improved motoneuron survival.

Ventral root avulsion injury typically occurs at the CNS-PNS interface, close to the cell body of the affected motoneurons, resulting in the death of the vast majority of motoneurons in the affected spinal segment (Gloviczki et al., 2017; Nógrádi and Vrbová, 2001; Pajer et al., 2014; Pajer et al., 2015). The injured motoneurons do not die instantaneously: after a latency period of 10 days a dramatic drop in the number of surviving motoneurons can be observed suggesting a marked vulnerability of the damaged cells to glutamate excitotoxicity (Koliatsos et al., 1994; Nógrádi et al., 2007; Van Den Bosch and Robberecht, 2000; Vandenberghe et al., 2000). The increased neuronal activity may reduce membrane clustering of KCC2 and thus Cl^- export (Chamma et al., 2013). This effect involves activation of NMDA receptors and subsequent Ca^{2+} influx, leading to de-phosphorylation of KCC2 Ser940 and calpain-dependent cleavage of the C-terminal domain of KCC2 (Chamma et al., 2013). Motoneurons can be successfully rescued by reducing glutamate excitotoxicity with riluzole treatment (Gloviczki et al., 2017; Nógrádi et al., 2007). It is an intriguing question whether a potent molecule such as riluzole, that acts through blocking voltage activated Na^+ and Ca^{2+} and activating K^+ channels and inhibits presynaptic glutamate release, is able to modulate the recovery of KCC2 expression in injured motoneurons. In fact, our confocal image analysis showed a significant decrease of KCC2 expression in the membranes of injured motoneurons between days 10 and 21 regardless of riluzole treatment following ventral root avulsion. On the other hand, the small, but significant difference in overall KCC2 expression detected between riluzole-treated and untreated specimens on postoperative days 10 and has likely derived from dendrites. It can be argued that the time course of KCC2 removal from the dendrites is slower in riluzole-treated animals. Indeed, the differential stability of dendritic versus somatic KCC2 in axotomized motoneurons has already been proposed by Akhter et al. (2019).

The results of confocal microscopy investigation of KCC2 expression in injured motoneurons were partly confirmed by dSTORM analysis. Super-resolution imaging provided a more detailed visualization of the cytoplasmic and membrane expression pattern of KCC2. While there was a continuous decrease in the membrane expression of KCC2 from day 5 to day 16 in the motoneurons of the riluzole-treated animals, a considerable increase followed by a sudden decrease could be observed in the cords of the untreated group. These results may suggest that decreased excitotoxicity by riluzole influences the membrane expression pattern of KCC2. These differential changes may be explained on a theoretical basis, supposing that either the existing KCC2 protein and transcript reserves are transiently mobilized until the gene expression is completely blocked at later time points, or a breakdown of KCC2 + clusters occurs in the membrane. As these interpretations are only theoretical at present, further studies are required to elucidate the exact mechanisms behind these complex and diverse phenomena found with a variety of methods. However, it should be considered that dSTORM analysis of individual sets of motoneurons leads to mapping of KCC2 expression alterations in a diverse set of motoneurons in the injured cords, as some motoneurons may survive the ventral root injury without treatment while other injured motoneurons remain non-responsive to riluzole treatment and die eventually. This is particularly true for spinal cords up to 10 days after injury, when it cannot be decided which motoneuron will die or survive at a later time point (Nógrádi et al., 2007).

It is well known that nerve injury results in increased NMDAR activity leading to Ca^{2+} influx, and a subsequent increase in intracellular Ca^{2+} concentrations (Jaiswal, 2014). The activity-dependent degradation of plasma membrane expression of KCC2 requires a Ca^{2+}-dependent signaling pathway that mediates functional activity of KCC2 (Kim et al., 2011). It could be hypothesized that an increase in intracellular Ca^{2+} level is directly associated with a decrease in KCC2 expression. However, increased intracellular Ca^{2+} density could be observed only in the untreated injured group at 5 days after the injury. Our electron microscopic investigations of electron-dense Ca^{2+} deposits provided clearcut evidence that most of the intracellularly accumulated Ca^{2+} localized to the mitochondria and led to the morphological and functional disorganization of these organelles and eventually to motoneuron death in the untreated *AV* animals. In contrast, in riluzole-treated motoneurons the intracellular/mitochondrial density of Ca^{2+} deposits were s similar to that of the contralateral intact motoneurons. This finding suggests that KCC2 expression levels in injured motoneurons were not directly influenced by elevated Ca^{2+} levels, but other, Ca^{2+}-independent signaling pathways may have been acting in these motoneurons. The regulation of KCC2 activity is mediated by numerous signaling pathways including trophic factors, phosphorylation, Zn^{2+} and direct interaction with other proteins (Chorin et al., 2011; Rivera et al., 2004; Shulga et al., 2012; Watanabe et al., 2009). Therefore, further studies are required to analyze the potential signaling pathways regarding the functional regulation of KCC2 following motoneuron injury.

Other interesting finding of this study was the expression pattern changes of EAAT-2 in the injured ventral horn. EAAT-2 is expressed in astrocytes (Allritz et al., 2010; Karki et al., 2014) and is responsible for the clearance of glutamate from the extracellular space thus facilitating glutamate uptake from the synaptic cleft (Allritz et al., 2010; Prydz et al., 2017). The down-regulation of EAAT-2 expression is associated with the pathogenesis of certain neurological disorders, eg. ALS (Hindeya Gebreyesus and Gebrehiwot Gebremichael, 2020). A considerable number of modulators (EGF, cAMP, PACAP, TGF-β, TNF-α, ceftriaxone, estrogen and neuronal soluble factors) reportedly modulate the expression of EAAT-2 via various signaling pathways (Todd and Hardingham, 2020).

The intriguing question remains, whether the results presented in this study can be aligned with the previous literature data concerning expression changes of KCC2 following cranial or peripheral nerve injuries with a possible restoration of nerve function. It has to be noted that while avulsion injury of one or more ventral roots leads to the death of the majority of affected motoneurons, injury of a peripheral nerve applied far away from the cell body of the motoneuron induces only a temporary minor degeneration of these neurons. Moreover, recovery of function is likely in the affected motoneurons if their axons are given a chance to regenerate in the peripheral or cranial nerves. Earlier studies have shown that injury followed by a coaptation of the murine vagus (Kim et al., 2018) or hypoglossal (Tatetsu et al., 2012) nerves induces marked downregulation of KCC2 expression on postoperative days 7 and 14 with an incomplete recovery of expression by day 28. On the other hand, sciatic crush injury resulted in a considerable decrease of membrane-bound KCC2 expression paralled by immunohistochemically detectable internalization of KCC2 in the cytoplasm of wild-type mouse lumbar motoneurons by day 7 postoperatively (Mòdol et al., 2014). These results suggest that there are similar molecular mechanisms acting in motoneurons affected by both the avulsion and peripheral nerve injuries, although the reversibility and outcome of the pathological processes are strikingly different in the two models. Unfortunately, differences in the methodological approaches applied in the present and previous studies do not allow very strict comparison of these data.

Although the main focus of the present study was placed on the ventral horn and motoneurons, one may have expected minor changes in KCC2 immunoreactivity in the dorsal horn. Interestingly, our data showed that avulsion of the L4–L5 motor roots did not significantly alter the expression of KCC2 in the superficial posterior grey matter layers (laminae I-II). A depolarizing shift in Cl^- reversal potential reportedly occurred in lamina I neurons due to a reduction in KCC2 expression in these cells following peripheral nerve injury. Moreover, decreased expression of KCC2 in spinal cord dorsal horn neurons proved to be a major contributor to neuropathic pain (Coull et al., 2003). Along this line, previous studies provided evidence that a unilateral L5 ventral root transection in rats was sufficient to induce hyperalgesia (Obata et al., 2004; Sheth et al., 2002). Unilateral ventral root avulsion at the L6–S1 spinal levels induced allodynia in rats accompanied by inflammatory changes in the dorsal horn regions, suggesting that activated microglia may have altered neuronal excitability after such injury (Bigbee et al., 2017). According to our data it can be hypothesized that hyperalgesia or allodynia after ventral root avulsion may develop without significant changes of KCC expression levels in the dorsal horn and thus other factors may be responsible for the pathological somatosensory perception.

5. Conclusion

Our results suggest that the damaged motoneurons were actively down-regulating KCC2 from their membranes and riluzole had no considerable effect on this process. However, the decreased excitotoxicity induced by riluzole, or the recovery process due to the rescue of a large sum of motoneurons had some effect on the dynamic of KCC2 expression pattern changes in the injured motoneurons. These findings suggest that excitotoxicity and KCC2 expression are not linked processes in the pathomechanism of motoneuron damage and consequent cell death after ventral root avulsion injury. Accordingly, it appears obvious from our results that continuous KCC2 expression in the membranes of injured motoneurons is not essential for motoneuron survival. These findings suggest that ventral root avulsion-induced motoneuron death is not due to the dislocation of KCC2 from the membrane, but this change appears to be an inevitable consequence of the injury, no matter whether it occurs proximally or distally from the cell body. On the other hand, riluzole-treated damaged motoneurons were able to preserve their calcium buffering capacity and thus prevent pathological processes induced by abnormal calcium levels. For this reason, it can rather be hypothesized that a bidirectional crosstalk develops between astrocytes and damaged neurons, which favorably affects EAAT-2 expression in astrocytes.

Funding

The project has received funding from Hungarian Brain Research Program (2017-1.2.1-NKP-2017-00002 to ME), National Research, Development and Innovation Office (TKP2021-NVA-19 to ME) and OTKA/NKFIH (KLINO-117031 to AN). We are grateful to prof. Dr. Bertalan Dudás (Lake Erie College of Osteopathic Medicine, Erie, PA, USA) for the kind collaborative gift of pKCC and ChAT antibodies.

CRediT authorship contribution statement

Krisztián Pajer: Conceptualization, Methodology, Writing – original draft, Visualization, Project administration. **Tamás Bellák:** Investigation, Writing – Original Draft, Visualization. **Tímea Grósz:** Formal analysis. **Bernát Nógrádi:** Investigation. **Roland Patai:** Investigation. **József Sinkó:** Formal analysis. **Laurent Vinay:** Conceptualization, Methodology. **Sylvie Liabeuf:** Investigation. **Miklós Erdélyi:** Formal analysis. **Antal Nógrádi:** Conceptualization, Methodology, Resources, Writing – review & editing, Funding acquisition.

Declaration of Competing Interest

The authors declare that they have no known competing financial interests or personal relationships that could have appeared to influence the work reported in this paper.

Data Availability

Data will be made available on request.

Appendix A. Supporting information

Supplementary data associated with this article can be found in the online version at doi:10.1016/j.ejcb.2023.151317.

References

Akhter, E.T., Griffith, R.W., English, A.W., Alvarez, F.J., 2019. Removal of the potassium chloride co-transporter from the somatodendritic membrane of axotomized motoneurons is independent of BDNF/TrkB signaling but is controlled by neuromuscular innervation. eNeuro 6.

Allritz, C., Bette, S., Figiel, M., Engele, J., 2010. Comparative structural and functional analysis of the GLT-1/EAAT-2 promoter from man and rat. J. Neurosci. Res 88, 1234–1241.

Bigbee, A.J., Akhavan, M., Havton, L.A., 2017. Plasticity of select primary afferent projections to the dorsal horn after a lumbosacral ventral root avulsion injury and root replantation in rats. Front Neurol. 8, 291.

Blaesse, P., Airaksinen, M.S., Rivera, C., Kaila, K., 2009. Cation-chloride cotransporters and neuronal function. Neuron 61, 820–838.

Borgers, M., 1981. The role of calcium in the toxicity of the myocardium. Histochem J. 13, 839–848.

Borgers, M., De Brabander, M., Van Reempts, J., Awouters, F., Jacob, W.A., 1977. Intranuclear microtubules in lung mast cells of guinea pigs in anaphylactic shock. Lab Invest 37, 1–8.

Boulenguez, P., Liabeuf, S., Bos, R., Bras, H., Jean-Xavier, C., Brocard, C., Stil, A., Darbon, P., Cattaert, D., Delpire, E., Marsala, M., Vinay, L., 2010. Down-regulation of the potassium-chloride cotransporter KCC2 contributes to spasticity after spinal cord injury. Nat. Med. 16, 302–307.
Chamma, I., Heubl, M., Chevy, Q., Renner, M., Moutkine, I., Eugène, E., Poncer, J.C., Lévi, S., 2013. Activity-dependent regulation of the K/Cl transporter KCC2 membrane diffusion, clustering, and function in hippocampal neurons. J. Neurosci. 33, 15488–15503.
Chorin, E., Vinograd, O., Fleidervish, I., Gilad, D., Herrmann, S., Sekler, I., Aizenman, E., Hershfinkel, M., 2011. Upregulation of KCC2 activity by zinc-mediated neurotransmission via the mZnR/GPR39 receptor. J. Neurosci. 31, 12916–12926.
Coull, J.A., Boudreau, D., Bachand, K., Prescott, S.A., Nault, F., Sík, A., De Koninck, P., De Koninck, Y., 2003. Trans-synaptic shift in anion gradient in spinal lamina I neurons as a mechanism of neuropathic pain. Nature 424, 938–942.
Dargaei, Z., Bang, J.Y., Mahadevan, V., Khademullah, C.S., Bedard, S., Parfitt, G.M., Kim, J.C., Woodin, M.A., 2018. Restoring GABAergic inhibition rescues memory deficits in a Huntington's disease mouse model. Proc. Natl. Acad. Sci. USA 115, E1618–E1626.
Doble, A., 1996. The pharmacology and mechanism of action of riluzole. Neurology 47, S233–S241.
Doyon, N., Prescott, S.A., Castonguay, A., Godin, A.G., Kröger, H., De Koninck, Y., 2011. Efficacy of synaptic inhibition depends on multiple, dynamically interacting mechanisms implicated in chloride homeostasis. PLoS Comput. Biol. 7, e1002149.
Gloviczki, B., Török, D.G., Márton, G., Gál, L., Bodzay, T., Pintér, S., Nógrádi, A., 2017. Delayed Spinal Cord-Brachial Plexus Reconnection after C7 Ventral Root Avulsion: The Effect of Reinnervating Motoneurons Rescued by Riluzole Treatment. J. Neurotrauma 34, 2364–2374.
Gulyás, A.I., Sík, A., Payne, J.A., Kaila, K., Freund, T.F., 2001. The KCl cotransporter, KCC2, is highly expressed in the vicinity of excitatory synapses in the rat hippocampus. Eur. J. Neurosci. 13, 2205–2217.
Hindeya Gebreyesus, H., Gebrehiwot Gebremichael, T., 2020. The potential role of astrocytes in Parkinson's disease (PD). Med Sci. 8.
Jaiswal, M.K., 2014. Selective vulnerability of motoneuron and perturbed mitochondrial calcium homeostasis in amyotrophic lateral sclerosis: implications for motoneurons specific calcium dysregulation. Mol. Cell Ther. 2, 26.
Kahle, K.T., Staley, K.J., Nahed, B.V., Gamba, G., Hebert, S.C., Lifton, R.P., Mount, D.B., 2008. Roles of the cation-chloride cotransporters in neurological disease. Nat. Clin. Pr. Neurol. 4, 490–503.
Karki, P., Webb, A., Smith, K., Johnson, J., Lee, K., Son, D.S., Aschner, M., Lee, E., 2014. Yin Yang 1 is a repressor of glutamate transporter EAAT2, and it mediates manganese-induced decrease of EAAT2 expression in astrocytes. Mol. Cell Biol. 34, 1280–1289.
Kim, J., Kobayashi, S., Shimizu-Okabe, C., Okabe, A., Moon, C., Shin, T., Takayama, C., 2018. Changes in the expression and localization of signaling molecules in mouse facial motor neurons during regeneration of facial nerves. J. Chem. Neuroanat. 88, 13–21.
Kim, K., Lee, S.G., Kegelman, T.P., Su, Z.Z., Das, S.K., Dash, R., Dasgupta, S., Barral, P.M., Hedvat, M., Diaz, P., Reed, J.C., Stebbins, J.L., Pellecchia, M., Sarkar, D., Fisher, P.B., 2011. Role of excitatory amino acid transporter-2 (EAAT2) and glutamate in neurodegeneration: opportunities for developing novel therapeutics. J. Cell Physiol. 226, 2484–2493.
Koliatsos, V.E., Price, W.L., Pardo, C.A., Price, D.L., 1994. Ventral root avulsion: an experimental model of death of adult motor neurons. J. Comp. Neurol. 342, 35–44.
Lang-Lazdunski, L., Heurteaux, C., Vaillant, N., Widmann, C., Lazdunski, M., 1999. Riluzole prevents ischemic spinal cord injury caused by aortic crossclamping. J. Thorac. Cardiovasc Surg. 117, 881–889.
Lauriat, T.L., Schmeidler, J., McInnes, L.A., 2007. Early rapid rise in EAAT2 expression follows the period of maximal seizure susceptibility in human brain. Neurosci. Lett. 412, 89–94.
Lee, H.H., Walker, J.A., Williams, J.R., Goodier, R.J., Payne, J.A., Moss, S.J., 2007. Direct protein kinase C-dependent phosphorylation regulates the cell surface stability and activity of the potassium chloride cotransporter KCC2. J. Biol. Chem. 282, 29777–29784.
Lee, H.H., Deeb, T.Z., Walker, J.A., Davies, P.A., Moss, S.J., 2011. NMDA receptor activity downregulates KCC2 resulting in depolarizing GABAA receptor-mediated currents. Nat. Neurosci. 14, 736–743.
Lindå, H., Shupliakov, O., Ornung, G., Ottersen, O.P., Storm-Mathisen, J., Risling, M., Cullheim, S., 2000. Ultrastructural evidence for a preferential elimination of glutamate-immunoreactive synaptic terminals from spinal motoneurons after intramedullary axotomy. J. Comp. Neurol. 425, 10–23.
Maltese, A., Maugeri, F., Drago, F., Bucolo, C., 2005. Simple determination of riluzole in rat brain by high-performance liquid chromatography and spectrophotometric detection. J. Chromatogr. B Anal. Technol. Biomed. Life Sci. 817, 331–334.
Maxwell, M.H., 1978. Two rapid and simple methods used for the removal of resins from 1.0 micron thick epoxy sections. J. Microsc. 112, 253–255.
Mayhew, T.M., 1992. A review of recent advances in stereology for quantifying neural structure. J. Neurocytol. 21, 313–328.
Meszlényi, V., Patai, R., Polgár, T.F., Nógrádi, B., Körmöczy, L., Kristóf, R., Spisák, K., Tripolszki, K., Széll, M., Obál, I., Engelhardt, J.I., Siklós, L., 2020. Passive transfer of sera from ALS patients with identified mutations evokes an increased synaptic vesicle number and elevation of calcium levels in motor axon terminals, similar to sera from sporadic patients. Int J. Mol. Sci. 21.
Mòdol, L., Mancuso, R., Alé, A., Francos-Quijorna, I., Navarro, X., 2014. Differential effects on KCC2 expression and spasticity of ALS and traumatic injuries to motoneurons. Front Cell Neurosci. 8, 7.
Nabekura, J., Ueno, T., Okabe, A., Furuta, A., Iwaki, T., Shimizu-Okabe, C., Fukuda, A., Akaike, N., 2002. Reduction of KCC2 expression and GABAA receptor-mediated excitation after in vivo axonal injury. J. Neurosci. 22, 4412–4417.
Nógrádi, A., Vrbová, G., 2001. The effect of riluzole treatment in rats on the survival of injured adult and grafted embryonic motoneurons. Eur. J. Neurosci. 13, 113–118.
Nógrádi, A., Szabó, A., Pintér, S., Vrbová, G., 2007. Delayed riluzole treatment is able to rescue injured rat spinal motoneurons. Neuroscience 144, 431–438.
Obál, I., Engelhardt, J.I., Siklós, L., 2006. Axotomy induces contrasting changes in calcium and calcium-binding proteins in oculomotor and hypoglossal nuclei of Balb/c mice. J. Comp. Neurol. 499, 17–32.
Obál, I., Nógrádi, B., Meszlényi, V., Patai, R., Ricken, G., Kovacs, G.G., Tripolszki, K., Széll, M., Siklós, L., Engelhardt, J.I., 2019. Experimental motor neuron disease induced in mice with long-term repeated intraperitoneal injections of serum from ALS patients. Int. J. Mol. Sci. 20.
Obata, K., Yamanaka, H., Dai, Y., Mizushima, T., Fukuoka, T., Tokunaga, A., Yoshikawa, H., Noguchi, K., 2004. Contribution of degeneration of motor and sensory fibers to pain behavior and the changes in neurotrophic factors in rat dorsal root ganglion. Exp. Neurol. 188, 149–160.
Paizs, M., Engelhardt, J.I., Katarova, Z., Siklós, L., 2010. Hypoglossal motor neurons display a reduced calcium increase after axotomy in mice with upregulated parvalbumin. J. Comp. Neurol. 518, 1946–1961.
Pajer, K., Feichtinger, G.A., Márton, G., Sabitzer, S., Klein, D., Redl, H., Nógrádi, A., 2014. Cytokine signaling by grafted neuroectodermal stem cells rescues motoneurons destined to die. Exp. Neurol. 261, 180–189.
Pajer, K., Nemes, C., Berzsenyi, S., Kovács, K.A., Pirity, M.K., Pajenda, G., Nógrádi, A., Dinnyés, A., 2015. Grafted murine induced pluripotent stem cells prevent death of injured rat motoneurons otherwise destined to die. Exp. Neurol. 269, 188–201.
Pintér, S., Gloviczki, B., Szabó, A., Márton, G., Nógrádi, A., 2010. Increased survival and reinnervation of cervical motoneurons by riluzole after avulsion of the C7 ventral root. J. Neurotrauma 27, 2273–2282.
Plantier, V., Sanchez-Brualla, I., Dingu, N., Brocard, C., Liabeuf, S., Gackière, F., Brocard, F., 2019. Calpain fosters the hyperexcitability of motoneurons after spinal cord injury and leads to spasticity. Elife 8.
Prescott, S.A., Sejnowski, T.J., De Koninck, Y., 2006. Reduction of anion reversal potential subverts the inhibitory control of firing rate in spinal lamina I neurons: towards a biophysical basis for neuropathic pain. Mol. Pain. 2, 32.
Prydz, A., Stahl, K., Puchades, M., Davarpaneh, N., Nadeem, M., Ottersen, O.P., Gundersen, V., Amiry-Moghaddam, M., 2017. Subcellular expression of aquaporin-4 in substantia nigra of normal and MPTP-treated mice. Neuroscience 359, 258–266.
Reynolds, E.S., 1963. The use of lead citrate at high pH as an electron-opaque stain in electron microscopy. J. Cell Biol. 17, 208–212.
Richardson, K.C., Jarett, L., Finke, E.H., 1960. Embedding in epoxy resins for ultrathin sectioning in electron microscopy. Stain Technol. 35, 313–323.
Rivera, C., Voipio, J., Thomas-Crusells, J., Li, H., Emri, Z., Sipilä, S., Payne, J.A., Minichiello, L., Saarma, M., Kaila, K., 2004. Mechanism of activity-dependent downregulation of the neuron-specific K-Cl cotransporter KCC2. J. Neurosci. 24, 4683–4691.
Rossi, D., Volterra, A., 2009. Astrocytic dysfunction: insights on the role in neurodegeneration. Brain Res. Bull. 80, 224–232.
Rothstein, J.D., Martin, L.J., Kuncl, R.W., 1992. Decreased glutamate transport by the brain and spinal cord in amyotrophic lateral sclerosis. N. Engl. J. Med 326, 1464–1468.
Rothstein, J.D., Martin, L., Levey, A.I., Dykes-Hoberg, M., Jin, L., Wu, D., Nash, N., Kuncl, R.W., 1994. Localization of neuronal and glial glutamate transporters. Neuron 13, 713–725.
Sánchez-Brualla, I., Boulenguez, P., Brocard, C., Liabeuf, S., Viallat-Lieutaud, A., Navarro, X., Udina, E., Brocard, F., 2018. Activation of 5-HT. Neuroscience 387, 48–57.
Schwartz, G., Fehlings, M.G., 2001. Evaluation of the neuroprotective effects of sodium channel blockers after spinal cord injury: improved behavioral and neuroanatomical recovery with riluzole. J. Neurosurg. 94, 245–256.
Sheth, R.N., Dorsi, M.J., Li, Y., Murinson, B.B., Belzberg, A.J., Griffin, J.W., Meyer, R.A., 2002. Mechanical hyperalgesia after an L5 ventral rhizotomy or an L5 ganglionectomy in the rat. Pain 96, 63–72.
Shulga, A., Magalhães, A.C., Autio, H., Plantman, S., di Lieto, A., Nykjær, A., Carlstedt, T., Risling, M., Arumäe, U., Castrén, E., Rivera, C., 2012. The loop diuretic bumetanide blocks posttraumatic p75NTR upregulation and rescues injured neurons. J. Neurosci. 32, 1757–1770.
Sinkó, J., Kákonyi, R., Rees, E., Metcalf, D., Knight, A.E., Kaminski, C.F., Szabó, G., Erdélyi, M., 2014. TestSTORM: Simulator for optimizing sample labeling and image acquisition in localization based super-resolution microscopy. Biomed. Opt. Express 5, 778–787.
Spejo, A.B., Oliveira, A.L., 2015. Synaptic rearrangement following axonal injury: Old and new players. Neuropharmacology 96, 113–123.
Szabadics, J., Varga, C., Molnár, G., Oláh, S., Barzó, P., Tamás, G., 2006. Excitatory effect of GABAergic axo-axonic cells in cortical microcircuits. Science 311, 233–235.
Tanaka, K., Watase, K., Manabe, T., Yamada, K., Watanabe, M., Takahashi, K., Iwama, H., Nishikawa, T., Ichihara, N., Kikuchi, T., Okuyama, S., Kawashima, N., Hori, S., Takimoto, M., Wada, K., 1997. Epilepsy and exacerbation of brain injury in mice lacking the glutamate transporter GLT-1. Science 276, 1699–1702.
Tatetsu, M., Kim, J., Kina, S., Sunakawa, H., Takayama, C., 2012. GABA/glycine signaling during degeneration and regeneration of mouse hypoglossal nerves. Brain Res. 1446, 22–33.
Todd, A.C., Hardingham, G.E., 2020. The regulation of astrocytic glutamate transporters in health and neurodegenerative diseases. Int. J. Mol. Sci. 21.

Toyoda, H., Ohno, K., Yamada, J., Ikeda, M., Okabe, A., Sato, K., Hashimoto, K., Fukuda, A., 2003. Induction of NMDA and GABAA receptor-mediated Ca2+ oscillations with KCC2 mRNA downregulation in injured facial motoneurons. J. Neurophysiol. 89, 1353–1362.

Van Den Bosch, L., Robberecht, W., 2000. Different receptors mediate motor neuron death induced by short and long exposures to excitotoxicity. Brain Res Bull. 53, 383–388.

Vandenberghe, W., Robberecht, W., Brorson, J.R., 2000. AMPA receptor calcium permeability, GluR2 expression, and selective motoneuron vulnerability. J. Neurosci. 20, 123–132.

Watanabe, M., Wake, H., Moorhouse, A.J., Nabekura, J., 2009. Clustering of neuronal K +-Cl- cotransporters in lipid rafts by tyrosine phosphorylation. J. Biol. Chem. 284, 27980–27988.

Williams, J.R., Sharp, J.W., Kumari, V.G., Wilson, M., Payne, J.A., 1999. The neuron-specific K-Cl cotransporter, KCC2. Antibody development and initial characterization of the protein. J. Biol. Chem. 274, 12656–12664.

Wyffels, J.T., 2001. Principles and techniques of electron microscopy: biological applications (by). In: Hayat., M.A. (Ed.), Microsc Microanal, Fourth ed., 7, p. 66 (by).